Nonergodicity in silo unclogging: Broken and unbroken arches

B. V. Guerrero,[1,*] B. Chakraborty,[2] I. Zuriguel,[1] and A. Garcimartín[1]
[1]*Dep. Física y Mat. Apl., Fac. Ciencias, Universidad de Navarra, 31080 Pamplona, Spain*
[2]*Martin Fisher School of Physics, Brandeis University, Waltham, Massachusetts 02454, USA*

(Received 15 May 2019; published 4 September 2019)

We report an experiment on the unclogging dynamics in a two-dimensional silo submitted to a sustained gentle vibration. We find that arches present a jerking motion where rearrangements in the positions of their beads are interspersed with quiescent periods. This behavior occurs for both arches that break down and those that withstand the external perturbation: Arches evolve until they either collapse or get trapped in a stable configuration. This evolution is described in terms of a scalar variable characterizing the arch shape that can be modeled as a continuous-time random walk. By studying the diffusivity of this variable, we show that the unclogging is a weakly nonergodic process. Remarkably, arches that do not collapse explore different configurations before settling in one of them and break ergodicity much in the same way than arches that break down.

DOI: 10.1103/PhysRevE.100.032901

I. INTRODUCTION

Dense flows of discrete bodies through a narrow orifice (a few times wider than particles) can be spontaneously arrested due to the emergence of arches spanning across the outlet. The archetypal example of clogging is the discharge of grains from a silo through an orifice at the bottom [1–7]. Clogging appears in many different systems, including colloidal suspensions, emulsions, active matter, and even living beings [8–11]. A clog is caused by geometrical and mechanical constrains, involving—among other variables—the ratio between orifice and particle size [12,13], grain stiffness [9,14] and shape [15–18], the shape of the hopper [19,20], and even the location and shape of a rigid obstacle above the outlet [21–23].

Applying an external vibration is one of the most commonly used mechanisms to burst the arches that stop the flow [24,25]. The vibration disturbs the granular medium and can resume the flow, just as thermal fluctuations in colloidal systems do [11]. Thus, the creation and destruction of arches during the discharge makes the flow intermittent. The duration of flow intervals follows an exponential distribution, whereas the distribution of the time intervals in which the system was clogged displays a heavy tail. The latter distribution depends mainly on the vibration intensity, the outlet size, and the load on the arch [8]. In general, a higher vibration breaks the arches more easily [24,26], but if it is too strong, it may induce a random motion of the grains that could increase the resistance to flow [27], just as a strong thermal noise does [11]. Hence, the design of a suitable and effective protocol requires a deep knowledge of the unclogging process.

To shed light on this problem, Lozano and coworkers studied how vibration affects the arch stability [26,28]. They used a two-dimensional silo with a small orifice at the bottom. The silo was submitted to a vertical sinusoidal vibration of a fixed frequency and increasing amplitude, and the vibration amplitude at which arches were broken was determined. They also photographed the clogging arches, and they were able to show that their geometry heavily influences their stability. In particular, the focus was put on the angles subtended between three successive bead centers of the arch (called ϕ). It was reported that the arch endurance greatly depends on the maximum of those angles ($\phi_{\max}$), so the higher the maximum angle is, the easier it is to break the arch [28].

Furthering that line of research, Guerrero and coworkers [29,30] used the same experimental device and studied how arches evolve along time when they are perturbed with a gentle constant vibration. They tracked the position of the arch beads during the arch lifespan. In Ref. [30] was found that arches evolve displaying some large and sudden morphological rearrangements in their shape (*large* meaning that each of them entail a sizable proportion of the total deformation sustained by the arch before collapsing, and *sudden* meaning that this occurs in a short amount of time in comparison with the arch lifespan). These motions were called "bursts" and are alternated with periods of less activity, or "quiescent periods." The external vibration allowed arches to explore different transient stable configurations that tend to be more and more irregular. Eventually, arches either collapsed or remained trapped in a configuration, keeping the same shape until the experimental run was stopped. Also, in that work it was put forward that the standard deviation σ of all the angles in the arch is a good way to quantify the arch regularity: The higher the σ, the less regular the arch. This scalar variable is also able to describe the shape changes along time, revealing the irregular "stick-slip" dynamics taking place during the process. Based on the two-time autocorrelation function of σ and its mean-squared displacement, it was reported that the arch evolution displays aging, i.e., a history dependency.

Concurrently, numerical simulations performed by Merrigan and coworkers [31] captured quite faithfully the observed features of unclogging. They offered the notion that the

*Corresponding author: bguerrero.3@alumni.unav.es

stick-slip like dynamics appeared because the arches were exploring a landscape of shapes, each one having its own stability. Their analysis showed that the evolution of arches could be modeled as a continuous-time random walk (CTRW) of a variable accounting for the arch geometry. Shape changes would therefore correspond to jumps of the CTRW and quiescent times to the periods during which an arch remains in the same configuration. Arch breakage would take place if the boundary of the space of stable configurations is reached, and, consequently, breaking times could be described as a first passage time of that boundary. In addition, they confirmed the time dependency of the arch evolution by proving that there exists breaking of ergodicity, in the sense that ensemble averages of a physical observable (in this case the mean-squared displacement, MSD) do not match their long-time averages. Although this nonergodic behavior is indeed expected for a subdiffusive CTRW with a broad distribution of quiescent times, it is also compatible with other subdiffusive stochastic processes with different physical origins [32].

In this article, we analyze in more depth the unclogging phenomenon by looking at the temporal evolution [30] of arches formed in a silo submitted to a constant, gentle vibration. For the first time, the dynamics of unbroken arches (those that survive for the whole experimental run) are studied. The aim is to ascertain whether there exists any feature that can set apart the evolution of broken and unbroken arches. In this regard, by taking the time series $\sigma(t)$ as a stochastic variable, the ergodicity breaking for broken and unbroken arches is revisited. In particular, we investigate the applicability of the CTRW model suggested by the numerical work of Merrigan and coworkers [31].

The article is organized as follows. In Sec. II the experimental device is explained; in Sec. III the dynamics of different kinds of arches is described in terms of the probability distributions of measurable times; in Sec. IV a detailed analysis of the ergodicity breaking is presented; in Sec. V the applicability of a simple CTRW is discussed; and, finally, in Sec. VI some conclusions are given.

II. EXPERIMENTAL SETUP AND METHODS

The details of the experimental setup are provided in Refs. [26,30]. As shown in Fig. 1, it basically consists of a flat-bottomed two-dimensional silo, filled with spheres and mounted on top of an electromagnetic shaker used to deliver a vertical vibration. The silo is made with two transparent polycarbonate sheets (390 mm high × 80 mm wide), with a sandwiched steel frame (1-cm-wide and 1.2-mm-thick). The container is divided in two equal enclosures (180 mm high × 60 mm wide) by two opposite movable steel flanges, arranged in such a way that the gap between them forms an orifice of length D. Thus, it resembles an hourglass: the upper chamber is the silo itself and the lower one collects the discharged material.

The grains are nonmagnetic stainless steel spheres of diameter $d = 1 \pm 0.01$ mm. The outlet width is $D = 4.4\,d$. The perturbation is a constant sinusoidal vibration with a peak acceleration of 0.6 g, i.e., a maximum dimensionless acceleration $\Gamma = 4A\pi f^2/g = 0.6$, with g the gravity acceleration, A the amplitude of the vibration, and f the frequency (fixed at 105 Hz). All these conditions are chosen in order to obtain a sizable amount of arches able to withstand vibration for sufficiently long times. We do not study here the dependencies with perturbation strength and the orifice size; these have been explored, to a limited extent, numerically in Ref. [31].

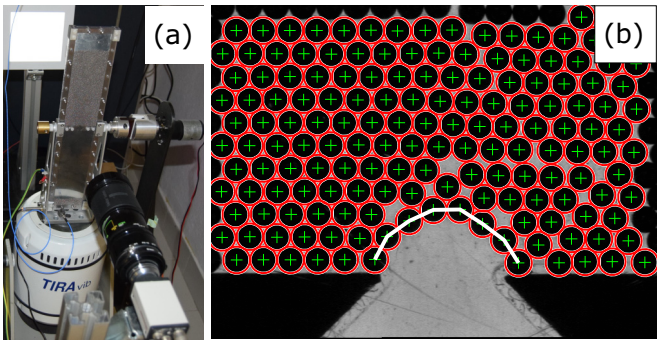

FIG. 1. (a) Bird's-eye view of the experimental setup. The silo is placed on top of the electromagnetic shaker and a camera located in front of a backlighted region near the silo outlet. (b) The result of the image processing. The center of each bead is detected (green cross marks) and the clogging arch is identified (solid white line).

The experimental procedure is fully automated with a software implemented by us in LabView. A charge coupled device (CCD) camera (placed in front of the backlighted silo) is used to record in a hard disk the region near the outlet at 25 frames per second. The experiment begins when the grains in the top reservoir start falling through the outlet by gravity. Real-time image analysis allows us to detect the moment when an arch is formed. Then the electromagnetic shaker is turned on to deliver the required external vibration and the camera records until the clog is destroyed (or until a time of 1200 s is reached). Afterward, the silo is rotated upside down with an electric motor. Next an intense vibration is applied until the silo is emptied. Finally, the container is rotated again to initiate another realization of an arch.

The processing stage of the video recordings is as follows. We first identify the center of each bead with a program that we wrote following the ideas of Shattuck and coworkers [33]. Essentially, we perform a convolution of the image with a disk of the same size than the particles, and locate the maxima of the convolution. Then, the arch is identified by determining the lowest chain of interconnected beads blocking the silo outlet, including the beads in contact with the base, as shown in Fig. 1(b). Afterward, the angles ϕ_i between the center of each bead in the arch and its two neighbors are measured. Then the arch irregularity is quantified by calculating the standard deviation σ of the angles ϕ_i. This procedure is repeated for all frames, so that finally the $\sigma(t)$ time series is obtained.

III. BREAKING, SETTLING, AND QUIESCENT TIME STATISTICS

The endurance of the arches submitted to vibrations is analyzed in terms of their breaking times t_b. Experimentally, t_b is calculated by subtracting the times corresponding to the last and the first images where the arch is identifiable. Instead of using the probability distribution function of breaking times,

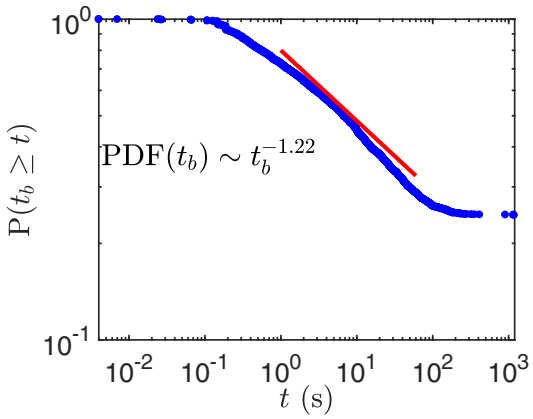

FIG. 2. Survival function of the breaking time t_b for $\Gamma = 0.6$, $f = 105$ Hz, $D = 4.4$. The power-law trend (solid red line) is a guide for the eye. Note the plateau after about 200 s and the high proportion of unbroken arches at the end of the experimental run.

$\mathrm{PDF}(t_b)$, we calculated the survival function which is the probability that an arch lasts longer than t and is defined as:

$$P(t_b \geqslant t) = \int_t^\infty \mathrm{PDF}(t')\, dt'. \tag{1}$$

Note that exponential or power-law PDFs will also have exponential or power-law survival functions, respectively.

Figure 2 shows the survival function of t_b for the population of arches analyzed in this work. Remarkably, the right censored events (i.e., arches that did not break before the maximum measurement time is reached) are plentiful (about 25% of all the arches, specifically 1093 of 4458 arches). This is displayed as a plateau at the right side of the survival function, a feature that has also been observed in similar experiments [8,26], although the right censored events were less abundant.

The $\mathrm{PDF}(t_b)$ corresponding to the observed survival function is heavy tailed. A power-law fit has been carried out for intermediate t_b (by using the method described in Ref. [34]) in order to compare our results with previous experiments [8,26], but it clearly fails to faithfully describe the data. Moreover, the plateau for long t_b implies that the average $\langle t_b \rangle$ diverges for long measurement times. It should be noted that if experiments are stopped early, then the plateau could go unnoticed. Some concepts, such as the proposed flowing-clogging transition [8,10,35], should be consequently revisited. Although a "clogged state" can be defined whenever $\langle t_b \rangle$ diverges, just taking into account the exponent from a fitted power law may not be enough.

An idea that can provide an explanation for these results is to consider that arches are not static entities. They evolve, changing their geometrical configuration, until a threshold is eventually reached that compromises their stability and the collapse occurs. This process can be described as a first passage time (FPT), that quantifies the time it takes for a random variable to reach a preset target or threshold for the first time [36]. In our case, the random variable would be $\sigma(t)$ and the target would be the breakage of the arch. In other words, $\mathrm{PDF}(t_b)$ would correspond to the FPT distribution of an absorbing boundary in a stable configuration space. This space consists of all the possible arch shapes, under the hypothesis that arch stability is only determined by its shape regardless of forces and memory effects.

The existence of a plateau in the distribution of Fig. 2 can be understood if one thinks that those arches have stopped exploring the configuration space because they have fallen into a very stable configuration, a "trap," from which they cannot escape. From a purely pragmatic point of view, if this is the case, then some additional absorbing states might be included in the FPT formalism. Our experimental data reveal some of these instances, such as the one shown in Fig. 3(a). It can be seen how the shape of the arch, as quantified by $\sigma(t)$, remains constant after a certain time. Let us call this

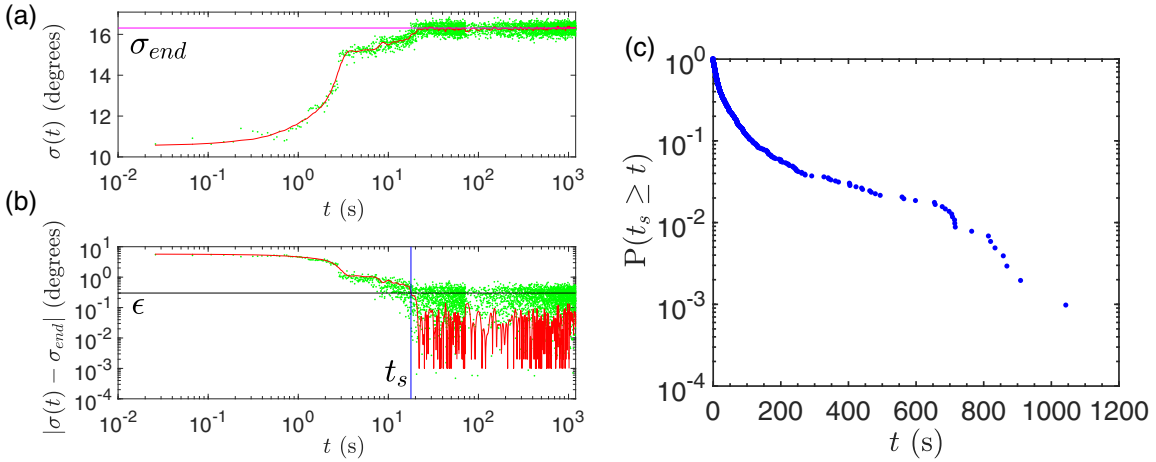

FIG. 3. (a) The evolution of the arch shape, as quantified by $\sigma(t)$ (green dots), for the arch shown in Fig. 1. The solid red line shows the filtered data and the horizontal magenta line σ_{end}. Note the logarithmic scale in the x axis. (b) The settling time t_s (blue vertical line) is calculated as the time elapsed from the start of the vibration to the moment when the filtered signal (red) falls below a given threshold $|\sigma(t) - \sigma_{\mathrm{end}}| \leqslant \epsilon$ and remains so until the end of the experiment. The value $\epsilon = 0.3$ has been used. Note that t_s is only measured for unbroken arches. (c) The survival function of settling times t_s for all the unbroken arches.

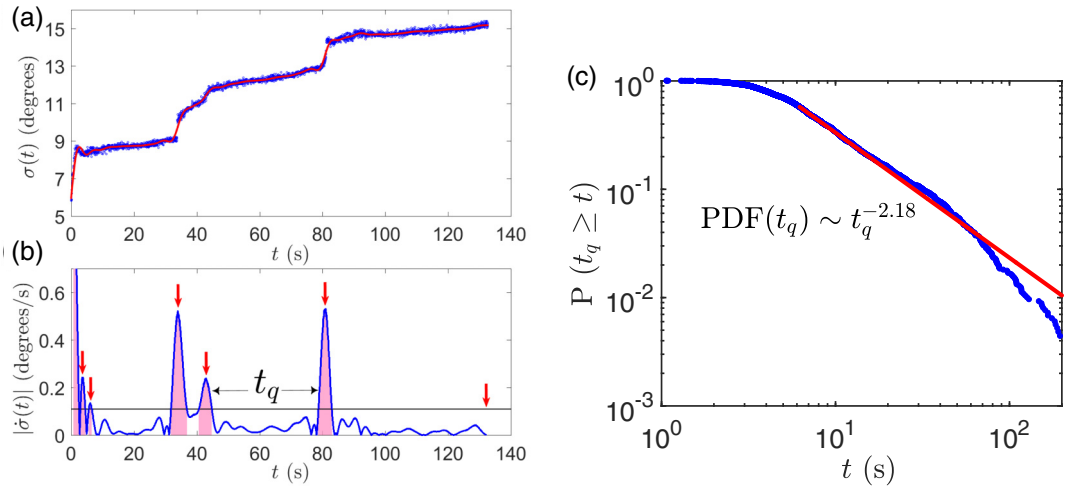

FIG. 4. (a) The shape evolution for an arch that breaks down after about 130 s, as quantified by $\sigma(t)$ (blue dots). The solid red line shows the filtered data. (b) Detection of burts for the filtered time series $\sigma(t)$ shown in (a). The threshold (horizontal black line) $|\dot{\sigma}(t)| = 0.11^\circ/\text{s}$ defines bursts (pink shaded area) and quiescent periods t_q (only one is shown). The red arrows indicate the peaks of activity for each burst detected. We consider that a new burst occurs if the time elapsed from the previous one (as measured between the maxima) is larger than 2 s. Notice that the breaking of the arch is also considered a burst. (c) Survival function of the quiescent times t_q between two successive bursts. The power-law trend (solid red line) is a guide for the eye.

value σ_{end}. This prompted us to define a settling time t_s as the moment when shape variations come to an end. Experimentally, we determine t_s as the time elapsed from the start of the vibration to the moment when $|\sigma(t) - \sigma_{\text{end}}|$ falls below an arbitrary threshold ϵ [see Fig. 3(b)] and remains below it until the end of the experiment. Although the choice of ϵ is to some extent arbitrary, PDF(t_s) is rather insensitive to ϵ (we have checked this with $\epsilon = 0.2^\circ$ and $\epsilon = 0.4^\circ$). We have obtained the survival function of settling times, $P(t_s \geqslant t)$, shown in Fig. 3(c), which seems to be broader than an exponential. The settling time t_s would correspond to the FPT associated to the additional absorbing states or traps. Note that from a theoretical point of view, these traps should not be considered an absorbing boundary, since arches could maybe escape from them. This differs from the arch breaking, which is obviously an irreversible event, well defined by an absorbing boundary.

The intermittent response to the gentle external perturbation can be characterized by the distribution of quiescent times t_q (see Fig. 4). Let us recall that quiescent times are intervals between large, sudden geometrical changes or "bursts." Figure 4(b) shows the detection of burst events for a given arch. In order to detect these bursts, the time series $\sigma(t)$ must be filtered to avoid false detections of local maxima resulting from the experimental noise. This smoothing [red line in Fig. 4(a)] was performed with a sixth-order Butterworth low-pass filter having a cutoff frequency of 0.25 Hz. We have tested cutoff frequencies of 0.125, 0.25, 0.375, and 0.625 Hz and did not observe significant changes in the main results. As the rearrangements take about 1 s [see Fig. 4(a)] the cutoff frequency of 0.25 Hz does not erase them but filters out the noise [see Fig. 3(a) and Fig. 4(a)]. We define a "burst" when the filtered signal grows faster than a preset threshold $\dot{\sigma}(t)$ and it occurs after more than 2 s from the previous one. In particular, we use the threshold $|\dot{\sigma}(t)| = 0.11^\circ/\text{s}$. The latency of 2 s, measured between the peaks of two consecutive events, is imposed to distinguish a rearrangement from the previous one: The impulse response of the filter lasts for a couple of seconds.

Figure 4(c) shows the survival function of t_q for arches that eventually break down. The choice of $\dot{\sigma} = 0.11^\circ/\text{s}$ is to some extent arbitrary but the PDF$(t_q > t)$ barely changes for values between $0.05^\circ/\text{s}$ and $0.20^\circ/\text{s}$. Note that t_q can be faithfully measured only for values much smaller than the maximum experimental time, and we have therefore set the limit at $t_q = 200$ s. As can be seen, the PDF(t_q) tail is broader than an exponential, so it lacks a characteristic timescale. For unbroken arches, the calculation of t_q is not trivial as it depends on how the settling time is defined and interpreted. One of the main issues when calculating the survival function for these arches is whether the time lapse after the settling time t_s should be included or not as a right censored event. Depending on the protocol used, it may introduce systematic errors that affect the tail of the estimated survival function. Anyway, Fig. 4 supports the notion that arch deformations, induced by a gentle vibration, are separated by quiescent times distributed with a broad PDF(t_q).

IV. ERGODICITY ANALYSIS

Aging is intrinsic to the glassylike behavior of the low-intensity vibration driven unclogging dynamics [30,31]. This time dependency naturally arises from subdiffusive stochastic processes [37,38]. Anomalous diffusion in a one-dimensional stochastic variable model is characterized by a nonlinear scaling of the MSD with time:

$$\text{MSD} = 2K_\alpha t^\alpha, \tag{2}$$

where K_α is a generalized diffusion coefficient and α is the MSD-based anomalous scaling exponent. Subdiffusion occurs for $0 < \alpha < 1$, Brownian motion for $\alpha = 1$, and superdiffusion for $\alpha > 1$.

Subdiffusive stochastic processes, characterized by an anomalous diffusion exponent $\alpha < 1$, usually entail a weak ergodicity breaking, in the sense that ensemble averages of a physical observable (such as the MSD) do not match their long-time averages [32]. For CTRW-based models, the key ingredient is the heavy-tailed distribution of quiescent times. However, non-CTRW models also lead to similar scaling laws for MSD. For instance, the scaled Brownian motion model (SBM) [37,39] relies on a time-dependent diffusivity while the heterogeneous diffusion processes (HDP) [40] consider a position-dependent diffusivity. A proper characterization of this anomalous self-diffusion could shed light on the transport properties in the heterogeneous environment where diffusion takes place.

In particular, we consider the $\Delta\sigma = \sigma(t) - \sigma(0)$ time series as an ensemble of random walkers moving in a phase space of stable arch configurations. Aiming to quantify to which extent is ergodicity broken for this process, we follow a method already used in granular systems [31,41]. We compute and compare both the ensemble-averaged mean-squared displacement (EAMSD) and the time-averaged mean-squared displacement (TAMSD).

A. Ensemble-averaged MSD

The EAMSD $\langle \Delta\sigma^2(t)\rangle$ is calculated as:

$$\langle \Delta\sigma^2(t)\rangle = \frac{1}{N(t)} \sum_{j=1}^{j=N(t)} \Delta\sigma(t)^2, \tag{3}$$

where angular brackets denote the ensemble average over the $N(t)$ surviving arches at time t. All arches have been taken into account regardless of the number of beads. Our population is dominated by arches with seven and eight beads, which account for about than 60% of the total.

The calculation of the EAMSD has been performed on four different sets of arches:

(i) Arches that remain unbroken after the maximum experimental time. Of course N does not change along time for this set. This group will be called unbroken arches (U).

(ii) Arches in the previous set (those that remain unbroken after the maximum experimental time) for which the dynamics has not stopped at time t. We will call them unsettled unbroken arches (UU).

(iii) Arches that will break before the maximum experimental time but still survive at time t. This set will be called broken arches (B).

(iv) All arches surviving at time t taken together. This ensemble will be called all arches (A).

The classification into these sets is done in order to analyze whether the diffusion differs or not for the different populations. We have considered the subset of unsettled unbroken arches with the aim to determine if their features are special among the whole set of unbroken arches (for instance, if they govern the diffusive behavior of all the unbroken arches). With this we intend to determine how the diffusive properties of the arches become affected by the existence of traps that arches cannot escape in order to distinguish if broken arches differ from unbroken ones.

Figure 5 shows the EAMSD of σ for the aforementioned sets. The most noticeable feature is that it behaves subdiffusively and for long times all the curves flatten. This might mean that the diffusion takes place in a bounded environment, a feature that may be related to the observation that there is a maximum amount of irregularity that arches can withstand [30].

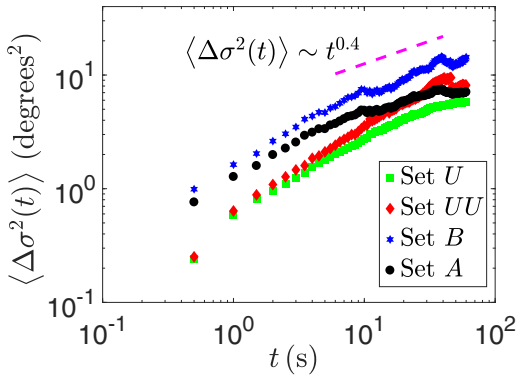

FIG. 5. Evolution of the ensemble-averaged MSD of σ $\langle \Delta\sigma^2(t)\rangle$. The initial sizes $N(t=0)$ for each group are 3365 broken arches (set B), 1093 unbroken arches (set U), 1031 unsettled unbroken arches (set UU), and a grand total of 4458 arches (set A). The scaling (dashed pink line) indicates the subdiffusive behavior trend for all the ensembles.

The trend displayed by both broken arches (set B) and unsettled unbroken arches (set UU) is quite similar. However, for all the arches (set A), the ensemble average $\langle \Delta\sigma^2(t)\rangle$ flattens more markedly after 10 s than it does for B and UU. This is necessarily caused by the contribution of arches that do not break and are settled in a stable configuration (that is, arches that do not belong in B or in UU). This is supported by the similar evolution of the EAMSD of the set of unbroken arches and the set of all arches (both flatten for long times).

B. Time-averaged MSD

The TAMSD is defined as [37]:

$$\overline{\delta_a^2(\Delta, T)} = \frac{1}{T-\Delta} \int_{t_a}^{T+t_a-\Delta} [\sigma(t'+\Delta) - \sigma(t')]^2 dt', \tag{4}$$

where the time average is performed for a time series $\sigma(t)$ over a time T as a function of the lag time Δ for an aging process initiated at $t = 0$ and measured from t_a onward. We will here consider the case $t_a = 0$, namely the measurement is started at the beginning of the aging process.

In Fig. 6 we show the evolution of the TAMSD of σ, $\overline{\delta_0^2(\Delta, T)}$, for individual arches lasting more than T and their ensemble-averaged TAMSD, $\langle \overline{\delta_0^2(\Delta, T)}\rangle$. In contrast to the EAMSD subdiffusive behavior, the ensemble-averaged TAMSD shows a diffusive or slightly supperdiffusive scaling for $\Delta \gtrsim 10$ s, as demostrated by the linear scaling (see red line in Fig. 7). Longer-time averages are not feasible with our experimental data.

C. Ergodicity breaking

The nonergodic behavior is demonstrated by the discrepancy between time and ensemble averages:

$$\left\langle \overline{\delta_0^2(\Delta, T)} \right\rangle \neq \langle \Delta\sigma^2(t)\rangle.$$

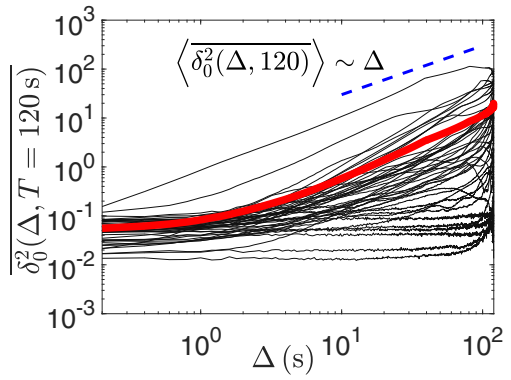

FIG. 6. Evolution of the time-averaged MSD of σ for individual arches (black lines) and their ensemble average (thick red line) for $T = 120$ s. The dashed blue line has a slope of 1, the value expected for weakly nonergodic processes.

The linear growth $\langle\overline{\delta_0^2(\Delta, T)}\rangle \simeq \Delta$ and the power-law growth $\langle\Delta\sigma^2(t)\rangle \simeq t^\alpha$ indicate that the unclogging phenomenon is weakly nonergodic, as reported in Ref. [31]. In particular, in some subdiffusive stochastic models for the weakly aged case, with $\{t_a, \Delta\} \ll T$, one would expect:

$$\left\langle\overline{\delta_0^2(\Delta, T)}\right\rangle \sim C\frac{\Delta}{T^{1-\alpha}}, \tag{5}$$

with a prefactor C depending on the model:

$$C = \begin{cases} \frac{2K_\alpha}{\Gamma(1+\alpha)}, & \text{for CTRW} \quad [42] \\ 2K_\alpha, & \text{for SBM} \quad [37] \\ \frac{\Gamma(\alpha+1/2)}{\sqrt{\pi}}\left(\frac{2}{\alpha}\right)^{2\alpha}(K_0)^\alpha, & \text{for HDP} \quad [40] \end{cases} \tag{6}$$

Note that in this formula $\Gamma(\cdot)$ is the Gamma function.

Figure 7 shows the scaling $\langle\overline{\delta_0^2(\Delta, T)}\rangle$ with T for different Δ for broken and for unsettled unbroken arches. Aging is

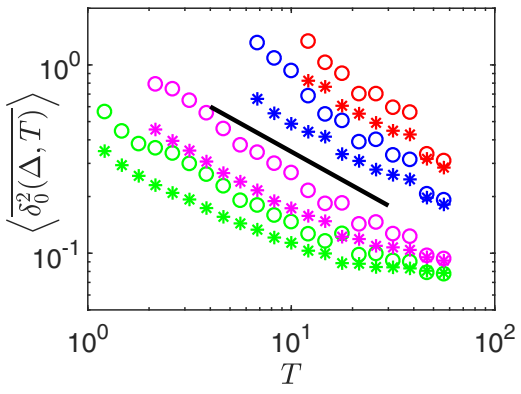

FIG. 7. Scaling of the ensemble-time-averaged MSD $\langle\overline{\delta_0^2(\Delta, T)}\rangle \sim \Delta/T^{1-\alpha}$ for different lag times Δ. Ensembles of broken arches, set B (circles), and unsettled unbroken arches, set UU (asterisks), were used. The colors indicate the used lag times: green for $\Delta = 0.5$ s, magenta for $\Delta = 1$ s, blue for $\Delta = 3$ s, and red for $\Delta = 5$ s. For a given T value, the ensemble-time-averaged MSD increases with Δ. The solid black line is $\sim T^{-0.6}$ or $T^{-1+\alpha}$ with $\alpha = 0.4$.

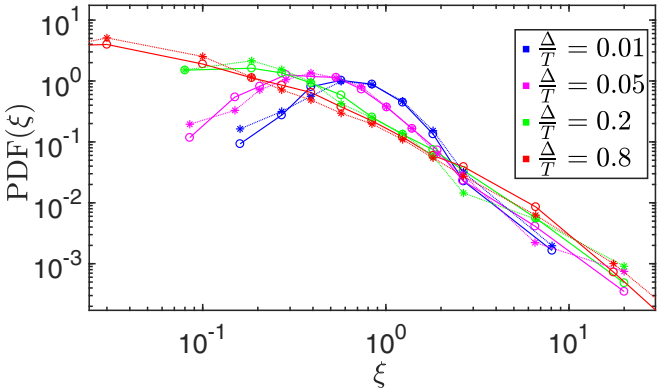

FIG. 8. Averaged PDF(ξ) for several Δ/T ratios (as indicated with color, see legend) using $T = \{5, 10, 30, 40, 50, 60, 100\}$ s and Δ ranging from 0.25 s to 80 s. Solid lines with circles are used for the broken arches and dotted lines with asterisks for the unsettled unbroken arches.

confirmed by the decrease of $\langle\overline{\delta_0^2(\Delta, T)}\rangle$ with T. The agreement with the relationship Eq. (5) strongly suggests that the unblocking phenomenon could be described in terms of a subdiffusive stochastic models, some of which are indicated in Eq. (6). Furthermore, the scaling is quite similar for both sets (B and UU), regardless of Δ. At first glance, the anomalous diffusion exponent α and the generalized diffusion coefficient K_α must have similar values for both. Slightly lower values are obtained for unbroken arches, meaning that a small difference in the effective diffusion coefficient K_α might exist, but it is irrelevant for practical purposes. On the whole, this hints that the nonergodic phase space exploration occurs much in the same way for both broken and unsettled unbroken arches.

D. Quantifying the breaking of ergodicity

Qualitatively, the relative broad scatter in $\overline{\delta_0^2(\Delta, T)}$ about $\langle\overline{\delta_0^2(\Delta, T)}\rangle$ (as displayed in Fig. 6) shows the expected ergodicity breaking. But even for ergodic systems, the statistical scatter of the amplitude of time-averaged quantities may stem from finite measurement times [43]. This scatter of the TAMSD around its mean can be characterized by the probability distribution of ξ, where the dimensionless variable ξ is

$$\xi(\Delta, T) = \frac{\overline{\delta^2(\Delta, T)}}{\langle\overline{\delta^2(\Delta, T)}\rangle}. \tag{7}$$

The PDF(ξ) is a good way to gauge whether the system is close to being ergodic. For an ergodic system, it will have a peak close to $\overline{\delta^2}/\langle\overline{\delta^2}\rangle = 1$, since the TAMSD and EAMSD are equivalent. Figure 8 shows PDF(ξ) for several Δ/T for both the sets of broken (empty circles) and unsettled unbroken arches (asterisks). The PDF(ξ) has been averaged over a range of T and Δ values. In agreement with previous works [31], it can be seen that the shape of PDF(ξ) is controlled by the ratio Δ/T: The lower the Δ/T ratio, the narrower the PDF(ξ) (meaning that the process is closer to being ergodic). PDF(ξ) for broken and for unsettled unbroken arches are quite similar,

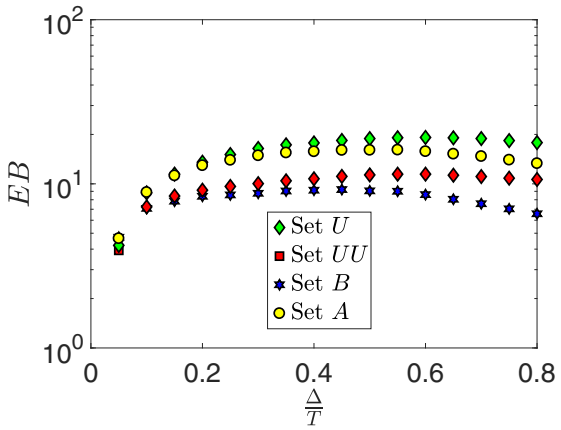

FIG. 9. EB as a function of Δ/T ratios, averaged over the measurement times $T = \{5; 10; 30; 40; 50; 60; 100\}$ s and Δ ranging from 0.25 s to 80 s for the different sets of arches.

which further supports our finding that these two sets undergo a similar process.

A better quantitative measure of the ergodic properties of a stochastic process is the ergodicity-breaking parameter, EB, defined as the variance of ξ; in other words, as the fourth moment of the TAMSD [42,43]:

$$\mathrm{EB} \equiv \langle \xi^2 \rangle - \langle \xi \rangle^2 = \frac{\langle (\overline{\delta^2})^2 \rangle - \langle \overline{\delta^2} \rangle^2}{\langle \overline{\delta^2} \rangle^2}. \tag{8}$$

For a subdiffusive continuous-time random walk, the EB parameter tends to the asymtotic value [42]:

$$\lim_{t\to\infty} \mathrm{EB} = \frac{2\Gamma^2(1+\alpha)}{\Gamma(1+2\alpha)} - 1, \tag{9}$$

where $\Gamma(\cdot)$ is the Gamma function. Although Eq. (9) is valid in the limit $\Delta/T \to 0$, it can be used for finite Δ/T ratios, regardless of Δ and K_α.

The parameter EB has been calculated for all the sets of arches as a function of Δ/T. This was done for $T = \{5, 10, 30, 40, 50, 60, 100\}$ s and Δ ranging from 0.25 to 80 s in order to see how much it depends on Δ/T. Figure 9 shows EB versus Δ/T for the four sets of arches. It can be seen that within the range $\Delta/T \in (0.2, 0.6)$, EB is roughly independent of Δ/T, as found in Ref. [31]. Note that the dependence of EB on Δ/T is quite similar for all the ensembles. It is worth stressing that EB has a value close to 10, which is not compatible with the value expected for a pure CTRW (EB < 1) nor for SBM and HDP [39,40]. The possible reasons of this mismatch are discussed in the next section.

V. APPLICABILITY OF A CTRW

Continuous time random walk models have been widely used to describe anomalous diffusion and aging [32,44]. In particular, Merrigan and coworkers used it to study a system quite similar to this one [31], and we will therefore discuss the validity of a simple CTRW to describe the results presented here. Arguably, the simplest case is the Scher-Montroll CTRW [45] that only relies on the basic assumption that random individual instantaneous jumps are separated by independent, random quiescent times t_q characterized by a distribution:

$$\mathrm{PDF}(t_q) \sim t_q^{-(1+\alpha)}. \tag{10}$$

For a subdiffusive CTRW, i.e., for $0 < \alpha < 1$, the average quiescent time $\langle t_q \rangle$ diverges. This divergence gives rise to the expected anomalous diffusion. In this case, the generalized diffusion coefficient [K_α in Eq. (2)] is [46]

$$K_\alpha = \frac{\langle \delta x^2 \rangle}{2\tau_0^\alpha}, \tag{11}$$

where $\langle \delta x^2 \rangle$ is the variance of the jump length and τ_0 is a characteristic timescale. Note that α comes from the distribution of quiescent times [Eq. (10)].

For a random walker $x(t)$ starting from $x = 0$, the distribution of times needed to reach a target x_0, known as the first-passage-time distribution $\wp(t)$, is [47]

$$\wp(t) \simeq \frac{x_0/K_\alpha^{1/2}}{t^{1+\alpha/2}}. \tag{12}$$

With the description provided by this CTRW model, the following scalings hold:

(i) $\mathrm{EAMSD}(\sigma) \sim t^\alpha$ grows subdiffusively,
(ii) $\mathrm{TAMSD}(\sigma) \sim \Delta$ grows diffusively,
(iii) $\langle \overline{\delta^2} \rangle \sim T^{1-\alpha}$.

Notice that other models apart from the CTRW are also able to explain the lack of ergodicity observed [32]. For instance, the SBM and the HDP models share the ensemble and time-averaged MSD scalings [including Eq. (5)]. The main difference is the underlying mechanism that gives rise to the nonergodic nature of the process: In the case of a CTRW it is due to a broad distribution of quiescent times that leads to the generalized diffusion coefficient given by Eq. (11); for an SBM, it is because of the time-dependent diffusion coefficient $K_\alpha(t) = \alpha K_\alpha t^{\alpha-1}$; and for the HDP it comes from the position-dependent diffusion coefficient $K_\alpha(x) \sim K_0|x|^{2/(2-\alpha)}$. In order to assess if any of these models may be eligible, it should be verified if α corresponds to any of these diffusion coefficients, as done in Ref. [41].

We have shown that the measured distributions of breaking times t_b and quiescent times t_q are heavy tailed. This supports the notion that the unclogging process could be modeled in terms of a one-dimensional CTRW of σ. If $\mathrm{PDF}(t_b)$ and $\mathrm{PDF}(t_q)$ were compatible with a Scher-Montroll CTRW description, then Eqs. (12) and (10) should be fulfilled, at least for the part where the distributions behave as a power law. Figures 2 and 4 support the notion that the arch dynamics can be described with a CTRW, in which the bursts are separated by quiescent times distributed with a broad $\mathrm{PDF}(t_q)$, in agreement with Ref. [31].

Going over our results and assuming that, at least for a range of time, the distribution tails of t_b and t_q scale as power laws, it would follow:

(a) $\mathrm{EAMSD}(\sigma) \sim t^{0.4}$
(b) $\mathrm{TAMSD}(\sigma) \sim \Delta$
(c) $\langle \overline{\delta^2} \rangle \sim T^{-0.6}$
(d) The value $\alpha \approx 0.4$ would give $\mathrm{PDF}(t_b) \sim t_b^{-1.2}$ after Eq. (12). This is compatible with the experimental measurements (at least for a given range of t_b, see Fig. 2).

Although these reasons seem to support that a simple CTRW can explain our results, two other facts reveal that either some ingredient is missing or a more complex model is required to capture the dynamics:

(a) PDF(t_q) $\sim t_q^{-2.2}$ (see Fig. 4), corresponding to $\alpha' \approx 1.2$, which is far from the expected $\alpha \approx 0.4$.

(a) EB ≈ 10 is an order of magnitude higher than the expected asymptotic value. For $\alpha = 0.4$, it should be EB ≈ 0.7 for a CTRW, which is close to the expected value for the SBM [39] and the HDP [40] models.

Clearly, $\alpha \not> 1$ in view of the verified weak ergodicity breaking. Although the exponent slightly depends on the arbitrary threshold used to calculate t_q, the disagreement is large enough to be caused by just an inaccurate choice. In fact, no subdiffusive exponent ($0 < \alpha < 1$) can account for the value EB ≈ 10, regardless of the PDF(t_q), which indicates that there must be another reason for the failing of this simple CTRW to faithfully reproduce the dynamics of the unclogging process.

In our experiments the time distributions are rather limited in time, covering at most two or three decades, which represents a handicap to test other CTRW models with more complex diffusive scalings. In fact, within our experimentally accessible time range it is not even possible to make out the short, intermediate, and long diffusion times, although we guess that our experiments would display a diffusive behavior for intermediate or large times.

Comparing with Merrigan's numerical results [31], our experiment confirms that the description can be simplified by considering a one-dimensional random walker, without losing the phenomenological richness of the unclogging process. By virtue of this, we were able to perform the ensemble averages without taking into account the number of beads in the arches, unlike them who only took arches with seven beads (which are the most prevalent, as in our case). Furthermore, our results provide a direct experimental measurement of PDF(t_q), whereas previously only a functional dependence was assumed. There is a remarkable agreement with their work. Both share the anomalous diffusion and the ergodicity breaking with a close quantitative agreement, even though there are small differences between our experiment and the numerically simulated system (such as the size and shape of the silo, the frequency and intensity of vibration applied, and grain friction).

VI. SUMMARY AND DISCUSSION

Arches that clog the silo output evolve intermittently before breaking when submitted to gentle vibrations, following a kind of irregular stick-slip motion. This evolution has been described in terms of $\sigma(t)$, a scalar variable that characterizes the arch shape. We observe how the arch beads undergo rearrangements and quantify them. The geometrical frustration hinders the free displacement from one configuration to another, leading to subdiffusion. This subdiffusive spreading is compatible with a heavy-tailed distribution of breaking times having a diverging timescale. The EAMSD of $\sigma(t)$ behaves subdiffusively, but the TAMSD displays normal diffusion. This mismatch between ensemble and time averages demonstrates the lack of ergodicity. Moreover, the ergodicity breaking was observed through the PDF(ξ) and quantitatively measured in terms of the EB parameter.

All this phenomenology can be rationalized in terms of a subdiffusive stochastic model as a CTRW with a heavy-tailed quiescent time distribution, as described in Ref. [31], but it is also compatible with scaled Brownian motion and heterogeneous diffusion process models. Nevertheless, the simple Scher-Montroll CTRW model, in which the quiescent times distribution is given by a a power law, is not enough to fully reproduce the measured quiescent times distribution and the ergodicity-breaking parameter, as reflected by the inconsistency of the α values.

The broader-than-power-law tails of escaping times (including the flattening of the heavy tails for long time) could be rationalized in terms of an energy trap model with a broader than exponential distribution of trap depths [48] or by assuming an alternative broader distribution of breaking times, at the expense of including a free parameter, as in Ref. [31]. An assortment of models more complex than the CTRW can be found in Refs. [37,38,44,49–53]; they could be useful to improve the description.

Let us also note that the stochastic dynamics for unbroken arches prior to their settling display the same behavior shown by the arches that eventually break. In fact, unsettled unbroken arches depart from the ergodicity much in the same way as broken arches do, suggesting that the settling of an unbroken arch in a trapped configuration occurs randomly during the exploration of configurations, regardless of the starting one. Our results also confirm the existence of aging, as recently demonstrated both in experiments and simulations.

Future experiments or simulations could be done using grains with different properties in order to analyze the interplay between static and dynamic friction, which can help to understand the observed glassy behavior. This system provides an ideal scenario to explore a simple frictional model [54] that could be used to explain the stick-slip-like dynamics. Indeed, this model might serve to rationalize, from physical principles, the origin of the broad time distributions and could lead to more realistic stochastic models.

The validity of future stochastic models proposals can be tested by revisiting the time distributions, MSD scalings, and ergodicity-breaking parameter. Besides, experiments or simulations where the stress on the arch can be measured (e.g., by using photoelastic disks) could explain the origin of the quiescent periods. From a more fundamental point of view, studying the physical origin of the jerking motion of vibrated arches opens a pathway to explore the local rheology (of the clogging beads and their vicinity) and how they influence the global rheological response [55], as well as the similarities with the flow of soft glassy materials [56]. This can be valuable to understand the reason for the diverging timescale near the clogging transition [57] and the nature of the unclogging phenomenon.

ACKNOWLEDGMENTS

This work was funded by Ministerio de Economía y Competitividad (Spanish Government) through Projects No. FIS2014-57325 and No. FIS2017-84631. B.C.'s work was

supported by NSF-CBET 1605428, and NSF-DMR 1409093. B.G. thanks Asociación de Amigos de la Universidad de Navarra for support through a scholarship. We also thank L. F. Urrea for technical help.

[1] J. Duran, *Sands, Powders, and Grains: An Introduction to the Physics of Granular Materials*, (Springer-Verlag, New York, 2000).
[2] H. Sakaguchi, E. Ozaki, and T. Igarashi, Int. J. Mod. Phys. B **07**, 1949 (1993).
[3] S. S. Manna and H. J. Herrmann, Euro. Phys. J. E **1**, 341 (2000).
[4] K. To, P. Y. Lai, and H. K. Pak, Phys. Rev. Lett. **86**, 71 (2001).
[5] I. Zuriguel, L. A. Pugnaloni, A. Garcimartín, and D. Maza, Phys. Rev. E **68**, 030301(R) (2003).
[6] S. Tewari, M. Dichter, and B. Chakraborty, Soft Matter **9**, 5016 (2013).
[7] C. C. Thomas and D. J. Durian, Phys. Rev. Lett. **114**, 178001 (2015).
[8] I. Zuriguel, D. R. Parisi, R. C. Hidalgo, C. Lozano, A. Janda, P. A. Gago, J. P. Peralta, L. M. Ferrer, L. A. Pugnaloni, E. Clément, D. Maza, I. Pagonabarraga, and A. Garcimartín, Sci. Rep. **4**, 7324 (2014).
[9] X. Hong, M. Kohne, M. Morrell, H. Wang, and E. R. Weeks, Phys. Rev. E **96**, 062605 (2017).
[10] G. A. Patterson, P. I. Fierens, F. Sangiuliano Jimka, P. G. König, A. Garcimartín, I. Zuriguel, L. A. Pugnaloni, and D. R. Parisi, Phys. Rev. Lett. **119**, 248301 (2017).
[11] R. C. Hidalgo, A. Goñi-Arana, A. Hernández-Puerta, and I. Pagonabarraga, Phys. Rev. E **97**, 012611 (2018).
[12] K. To and P. Y. Lai, Phys. Rev. E **66**, 011308 (2002).
[13] J. R. Valdes and J. C. Santamarina, Can. Geotech. J. **45**, 177 (2008).
[14] A. Ashour, T. Trittel, T. Börzsönyi, and R. Stannarius, Phys. Rev. Fluids **2**, 123302 (2017).
[15] J. Tang and R. P. Behringer, Eurphys. Lett. **114**, 34002 (2016).
[16] A. Ashour, S. Wegner, T. Trittel, T. Börzsönyi, and R. Stannarius, Soft Matter **13**, 402 (2017).
[17] J. Török, S. Lévay, B. Szabó, E. Somfai, S. Wegner, R. Stannarius, and T. Börzsönyi, EPJ Web Conf. **140**, 03076 (2017).
[18] E. Goldberg, C. M. Carlevaro, and L. A. Pugnaloni, J. Stat. Mech. - Theory Exp. (2018) 113201.
[19] H. G. Sheldon and D. J. Durian, Granular Matter **12**, 579 (2010).
[20] D. López-Rodríguez, D. Gella, K. To, D. Maza, A. Garcimartín, and I. Zuriguel, Phys. Rev. E **99**, 032901 (2019).
[21] I. Zuriguel, A. Janda, A. Garcimartín, C. Lozano, R. Arévalo, and D. Maza, Phys. Rev. Lett. **107**, 278001 (2011).
[22] K. Endo, K. A. Reddy, and H. Katsuragi, Phys. Rev. Fluids **2**, 094302 (2017).
[23] A. Vamsi Krishna Reddy, S. Kumar, K. Anki Reddy, and J. Talbot, Phys. Rev. E **98**, 022904 (2018).
[24] A. Janda, D. Maza, A. Garcimartín, E. Kolb, J. Lanuza, and E. Clément, Eurphys. Lett. **87**, 24002 (2009).
[25] C. Mankoc, A. Garcimartín, I. Zuriguel, D. Maza, and L. A. Pugnaloni, Phys. Rev. E **80**, 011309 (2009).
[26] C. Lozano, I. Zuriguel, and A. Garcimartín, Phys. Rev. E **91**, 062203 (2015).
[27] K. To and H.-T. Tai, Phys. Rev. E **96**, 032906 (2017).
[28] C. Lozano, G. Lumay, I. Zuriguel, R. C. Hidalgo, and A. Garcimartín, Phys. Rev. Lett. **109**, 068001 (2012).
[29] B. Guerrero, C. Lozano, I. Zuriguel, and A. Garcimartín, EPJ Web Conf. **140**, 03016 (2017).
[30] B. V. Guerrero, L. A. Pugnaloni, C. Lozano, I. Zuriguel, and A. Garcimartín, Phys. Rev. E **97**, 042904 (2018).
[31] C. Merrigan, S. K. Birwa, S. Tewari, and B. Chakraborty, Phys. Rev. E **97**, 040901(R) (2018).
[32] R. Metzler, J.-H. Jeon, A. G. Cherstvy, and E. Barkai, Phys. Chem. Chem. Phys. **16**, 24128 (2014).
[33] Shattuck, M. D. "Particle Tracking" [http://gibbs.engr.ccny.cuny.edu/technical/Tracking/ChiTrack.php (2008)].
[34] A. Clauset, C. R. Shalizi, and M. E. J. Newman, SIAM Rev. **51**, 661 (2009).
[35] C. C. Thomas and D. J. Durian, Phys. Rev. E **87**, 052201 (2013).
[36] S. Redner, *A Guide to First-Passage Processes* (Cambridge University Press, Cambridge, UK, 2001).
[37] H. Safdari, A. V. Chechkin, G. R. Jafari, and R. Metzler, Phys. Rev. E **91**, 042107 (2015).
[38] R. Hou, A. G. Cherstvy, R. Metzler, and T. Akimoto, Phys. Chem. Chem. Phys. **20**, 20827 (2018).
[39] F. Thiel and I. M. Sokolov, Phys. Rev. E **89**, 012115 (2014).
[40] A. G. Cherstvy and R. Metzler, Phys. Rev. E **90**, 012134 (2014).
[41] A. Bodrova, A. V. Chechkin, A. G. Cherstvy, and R. Metzler, Phys. Chem. Chem. Phys. **17**, 21791 (2015).
[42] Y. He, S. Burov, R. Metzler, and E. Barkai, Phys. Rev. Lett. **101**, 058101 (2008).
[43] M. Schwarzl, A. Godec, and R. Metzler, Sci. Rep. **7**, 3878 (2017).
[44] R. Kutner and J. Masoliver, Eur. Phys. J. B **90**, 50 (2017).
[45] H. Scher and E. W. Montroll, Phys. Rev. B **12**, 2455 (1975).
[46] R. Metzler and J. Klafter, Phys. Rep. **339**, 1 (2000).
[47] H. Krüsemann, A. Godec, and R. Metzler, Phys. Rev. E **89**, 040101(R) (2014).
[48] A. Nicolas, A. Garcimartín, and I. Zuriguel, Phys. Rev. Lett. **120**, 198002 (2018).
[49] S. Burov, J.-H. Jeon, R. Metzler, and E. Barkai, Phys. Chem. Chem. Phys. **13**, 1800 (2011).
[50] A. G. Cherstvy and R. Metzler, J. Chem. Phys. **142**, 144105 (2015).
[51] H. Safdari, A. G. Cherstvy, A. V. Chechkin, A. Bodrova, and R. Metzler, Phys. Rev. E **95**, 012120 (2017).
[52] A. V. Chechkin, H. Kantz, and R. Metzler, Eur. Phys. J. B **90**, 205 (2017).
[53] T. Akimoto, A. G. Cherstvy, and R. Metzler, Phys. Rev. E **98**, 022105 (2018).
[54] B. Blanc, J.-C. Géminard, and L. A. Pugnaloni, Eur. Phys. J. E **37**, 112 (2014).
[55] A. Ferguson and B. Chakraborty, Phys. Rev. E **73**, 011303 (2006).
[56] V. Mansard and A. Colin, Soft Matter **8**, 4025 (2012).
[57] H. Péter, A. Libál, C. Reichhardt, and C. J. O. Reichhardt, Sci. Rep. **8**, 10252 (2018).